COMMUNICATION

Plasma-Catalytic Reactions for Soot Oxidation on VO_x/M (M=KIT-6, SBA-15 and SiO_2) Catalysts: Influence of Pore Structure

Hanpeng Wu,[a] Xinbo Zhu,*[a] Xiqiang Wu,[a] Xin Tu,*[b] Geng Chen,[a] and Guohua Yang[a]

[a] H. Wu, Dr. X. Zhu, X. W, Dr. G. Chen, Prof. G. Yang
Faculty of Maritime and Transportation
Ningbo University
Ningbo, Zhejiang Province, 315211 China
E-mail: zhuxinbo@nbu.edu.cn
[b] Prof. X. Tu
Department of Electrical Engineering and Electronics
University of Liverpool
L69 3BX, Liverpool, UK
E-mail: Xin.Tu@liverpool.ac.uk

Abstract: In this work, the effect of pore structure for VO_x/M (M=KIT-6, SBA-15 and SiO_2) catalysts on plasma-catalytic soot oxidation was investigated. The combination of VO_x/KIT-6 and plasma shows the highest soot oxidation rate, followed by VO_x/SBA-15-packed and VO_x/SiO_2-packed plasma reactor. The soot oxidation rate of 97.4% and the energy efficiency of 0.95 g·kWh^{-1} can be achieved in the plasma-catalytic soot oxidation over VO_x/KIT-6 at 30th min and 20 W. The catalysts were characterized by Brunner-Emmet-Teller (BET), X-ray diffraction (XRD), transmission electron microscopy (TEM), Hydrogen temperature-programmed reduction (H_2-TPR) and X-ray Photoelectron Spectroscopy (XPS). The BET, XRD and TEM results illustrated that VO_x/KIT-6 and VO_x/SBA-15 had large specific surface areas and good dispersion of vanadium species. The H_2-TPR and XPS results confirmed that VO_x/KIT-6 had stronger reducibility and higher $O_{ads}/(O_{ads}+O_{latt})$ ratio than those of VO_x/SBA-15 and VO_x/SiO_2. The good performance of soot oxidation in the plasma-catalytic systems over VO_x/KIT-6 could be attributed to 1) the well-developed 3D mesoporous structure, which facilitated the transportation of radicals and active species, and 2) improved properties of VO_x/KIT-6, since more active sites and surface adsorbed oxygen species on the catalyst surfaces contributed to soot oxidation.

Introduction

Soot emissions from diesel engine have a negative impact on both atmospheric environment and human health. To meet the stringent legislations and reduce the soot emissions from diesel engine, great efforts have been devoted to the research and development of soot abatement technologies. Diesel particulate filter (DPF) is the most effective technology for soot emissions control.[1] The pores of DPF will be blocked by soot particles. Thus, the regeneration of DPF via soot oxidation is of great significance. However, conventional catalytic soot oxidation needs a high temperature (above 350 °C), which requires external heating source.[2]

Plasma-catalytic system provides a promising solution for soot oxidation at atmospheric pressure and below 250 °C. The interactions between plasma and catalysts could generate a synergistic effect in soot oxidation over MnO_x/CeO_2, that is, the active radicals produced by plasma could diffuse to the surface of MnO_x/CeO_2 catalyst, which could trigger more effective collisions between oxidative species and soot on catalyst surfaces.[3] Previous studies also showed that soot oxidation over MnO_x-CeO_2 catalyst could be launched below 240.8 °C with pulsed dielectric barrier discharge (DBD) plasma and the ignition temperature for soot oxidation will decrease with the increase of the pulse DBD frequencies.[4] The composition of catalysts has a significant effect on the reaction performance under the plasma environment. Ranji-Burachaloo et al.[5] found that the soot oxidation rates of MnO_x, Fe_2O_3 and Co_3O_4 were 90%, 85%, and 79%, respectively, in the plasma-catalytic soot oxidation experiments at 350 °C and 7.4 W.

Vanadium oxides are extensively used for hydrocarbon oxidation and selective catalytic reduction of NO_x.[6] Previous study showed that V/MCM-41 exhibited 10% higher conversion rate than MCM-41 supported the other transition-metal catalysts for the selective oxidation of cyclohexane to cyclohexanol.[7] The combination of plasma and V-W-Ti catalysts improved the removal rate of dimethyl sulfide by over 50% compared with the result of using plasma alone.[8] The sample of 4% VO_x/TiO_2 also exhibited good catalytic activity in soot oxidation, with T_{50} of 390 °C and T_{90} of 424 °C.[9]

Pore structure of the catalyst could impose an effect on catalytic activity. The well-developed pore structures are facilitated for the transportation of reactive species.[10] Sridevi et al.[11] reported that the cyclohexanol conversion rates of Cu/SBA-15 and Cu/KIT-6 reached nearly 70%, which were over 10% higher than that of Cu/SiO_2. Liu et al.[12] found that the glyoxal conversion of Pd/KIT-6 was 8.5% higher than that of Pd/SBA-15. At present, there are very few studies on the effect of mesoporous silica supports with different pore structures on soot oxidation, especially in the presence of plasma-induced reactions.

In this work, VO_x/M (M=KIT-6, SBA-15 and SiO_2) catalysts were synthesized using impregnation method. These catalysts were characterized by BET, XRD, TEM, H_2-TPR and XPS. The performance of plasma-catalytic soot oxidation was investigated in terms of the soot oxidation rate and energy efficiency, while the underlying mechanisms were discussed.

Results and Discussion

The contents of V in VO_x/M catalysts are 0.95, 1.03 and 0.94 wt.%, respectively. (Table 1) By comparison, the ICP analysis shows that V loading amount is close to the theoretical value of 1 wt.%. The physical properties of the samples are summarized in Table 1. The specific surface area (S_{BET}) of VO_x/KIT-6 (456 m^2·g^{-}

^{1}) and VO_x/SBA-15 (466 $m^2 \cdot g^{-1}$) are lower compared with pure KIT-6 (780 $m^2 \cdot g^{-1}$) and SBA-15 (575 $m^2 \cdot g^{-1}$), respectively. The average pore diameters of the samples are between 5.5 to 8.2 nm. These phenomena are caused by the introduction of vanadium species.[12] Compared to VO_x/SiO_2, both VO_x/KIT-6 and VO_x/SBA-15 catalysts possess higher S_{BET} and pore volume.

Figure 1 shows the XRD patterns of VO_x/M (M=KIT-6, SBA-15 and SiO_2) catalysts. The XRD patterns of all three catalysts maintain the characteristics diffraction peaks of the supports. The broad diffraction peaks at 22.2° in the XRD patterns of VO_x/KIT-6 and VO_x/SBA-15 could be attributed to the amorphous silica in pore wall.[13] The XRD diffraction peak of VO_x/SiO_2 is consistent with that of SiO_2 (PDF# 46-1045). No diffraction peak of vanadium species was detected over all three catalysts. This could be attributed to the good dispersion of vanadium species on supports, or relatively low loading amount of vanadium oxide species.[13-14] The XRD patterns of the used VO_x/M catalysts are presented in Figure S3 (see in the Supporting Information). No distinct changes are observed in the XRD patterns of fresh and used VO_x/M catalysts, indicating that VO_x/M catalysts still maintain the crystal structure of the supports after plasma-catalytic soot oxidation.

Table 1. Physicochemical properties of VO_x/M (M=KIT-6, SBA-15 and SiO_2) catalysts.

Catalyst	The contents of V (wt.%)[a]	S_{BET} ($m_2 \cdot g^{-1}$)	V_{pore} ($cm^3 \cdot g^{-1}$)	d_{pore} (nm)
VO_x/KIT-6	0.95	456	0.84	7.4
VO_x/SBA-15	1.03	466	0.95	8.2
VO_x/SiO_2	0.94	10	0.01	5.5

[a] Measured by ICP.

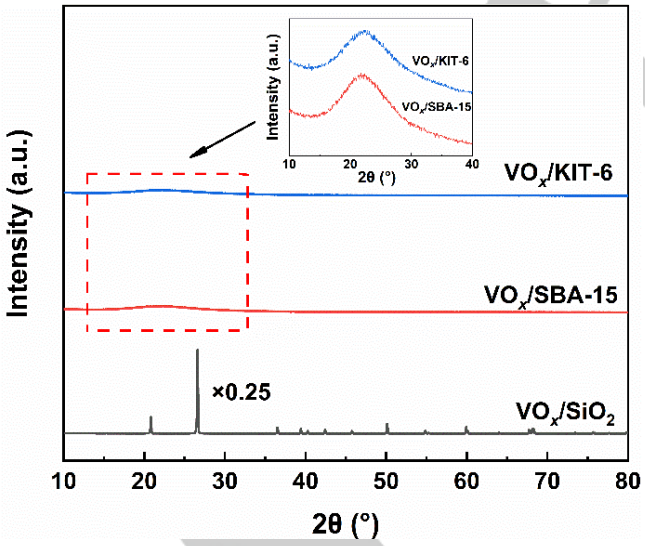

Figure 1. XRD patterns of VO_x/M (M=KIT-6, SBA-15 and SiO_2) catalysts.

TEM images of VO_x/M (M=KIT-6, SBA-15 and SiO_2) catalysts are shown in Figure 2. The well-ordered mesoporous structure of KIT-6 and SBA-15 supports could be clearly visible from the TEM images of VO_x/KIT-6 and VO_x/SBA-15 catalysts (Figure 1a, c), which are in consistent with previous literature.[15] This indicates that the introduction of vanadium species does not change the well-ordered mesoporous of KIT-6 and SBA-15. As shown in Figure 2, small particles of vanadium species could be observed on the surface of VO_x/M (M=KIT-6, SBA-15 and SiO_2) catalysts in the TEM images. This indicates that particles of vanadium species are very well dispersed on the surface of catalysts, in consistent with the XRD results.[13] In Figure 1(b), (d), (f), the detected lattice fringe with a lattice spacing of 0.29 nm belongs to the crystal phases (3 0 1) to V_2O_5 crystals (PDF# 41-1426) well, confirming that vanadium species exist on the surface of KIT-6, SBA-15 and SiO_2 supports.

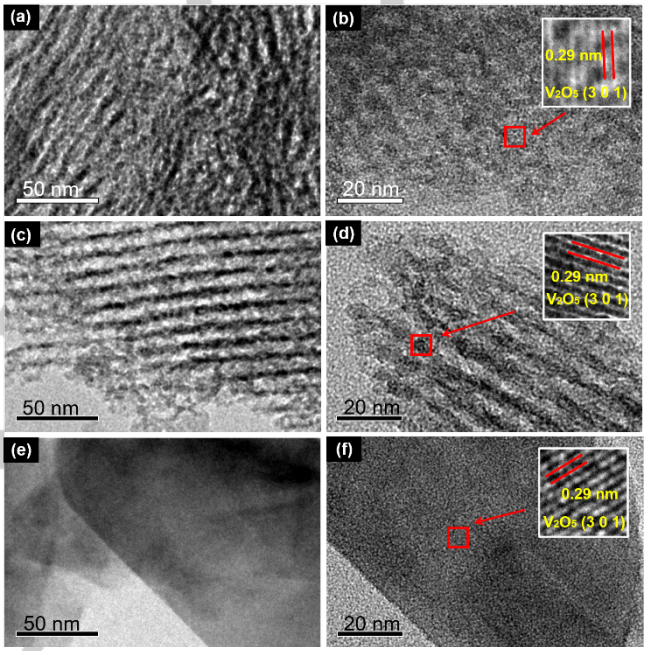

Figure 2. TEM images of VO_x/M (M=KIT-6, SBA-15 and SiO_2) catalysts: (a) and (b) VO_x/KIT-6; (c) and (d) VO_x/SBA-15; (e) and (f) VO_x/SiO_2.

Figure 3 is the H_2-TPR profiles of VO_x/M (M=KIT-6, SBA-15 and SiO_2) catalysts. A major reduction peak can be observed in all H_2-TPR profiles, which can be attributed to the reduction of V^{5+} to V^{3+} species.[16] The reduction temperature of the VO_x/KIT-6 and VO_x/SBA-15 shift to lower temperatures (478 °C, 483 °C) compared with VO_x/SiO_2 (556 °C), indicating improved reducibility of the VO_x/M catalysts using KIT-6 and SBA-15 as the support. The H_2 consumption amount of VO_x/KIT-6 is higher than that of VO_x/SBA-15 (Table 2), indicating more surface adsorbed oxygen species on the surface of VO_x/KIT-6. The higher reducibility of VO_x/KIT-6 may benefit its catalytic performance for the soot oxidation.[14]

Figure 4 shows the XPS spectra for O 1s of VO_x/M (M=KIT-6, SBA-15 and SiO_2) before and after plasma-catalytic soot oxidation. The peaks at the binding energy of 531.3~532.2 eV belong to lattice oxygen (denoted as O_{latt}), while the peaks at 532.7~533.5 eV could be attributed to surface adsorbed oxygen (denoted as O_{ads}).[17] $O_{ads}/(O_{ads}+O_{latt})$ radios of the fresh VO_x/M catalysts are shown in Table 2. The $O_{ads}/(O_{ads}+O_{latt})$ ratios of VO_x/KIT-6 and VO_x/SBA-15 are 58.8% and 49.7%, respectively, which are significantly greater than 30.8% of VO_x/SiO_2. The

relative concentration of O_{ads} is closely associated with catalytic activity, since the O_{ads} is much easier to be activated for the surface reactions due to its higher mobility.[6a, 17-18] VO_x/KIT-6 with abundant O_{ads} on the surface is promising to improve soot oxidation. After reaction, the $O_{ads}/(O_{ads}+O_{latt})$ ratios decrease to 49.3% for VO_x/KIT-6 and 41.5% for VO_x/SBA-15, respectively, which are much larger than 24.6% of VO_x/SiO_2. (Table S1) This phenomenon indicates that O_{ads} on the catalysts surface is consumed during the process of plasma-catalytic soot oxidation.[19] The higher content of the O_{ads} could be beneficial to produce more active oxygen species.[20] The highest O_{ads} consumption of VO_x/KIT-6 indicates that it can produce more active oxygen species and has better catalytic activity in the plasma-catalytic soot oxidation.

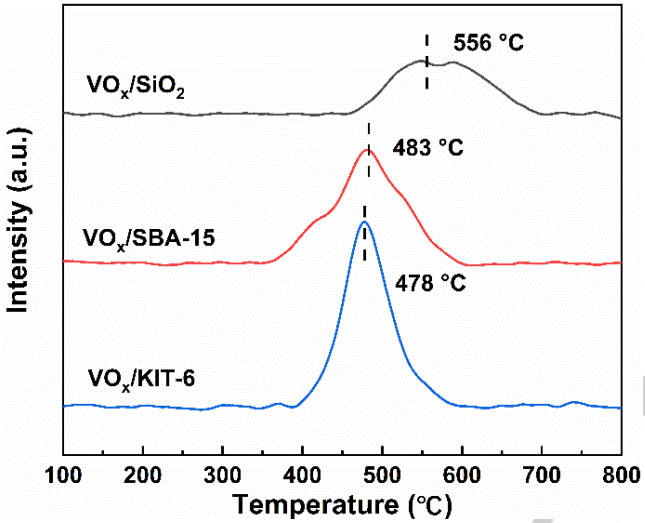

Figure 3. H_2-TPR profiles of VO_x/M (M=KIT-6, SBA-15 and SiO_2) catalysts.

Table 2. H_2 consumption and XPS parameters of VO_x/M (M=KIT-6, SBA-15 and SiO_2) catalysts.

Catalyst	H_2 consumption ($mmol \cdot g^{-1}$)	$O_{ads}/(O_{ads}+O_{latt})$ (%)
VO_x/KIT-6 (Fresh)	0.15	58.8
VO_x/SBA-15 (Fresh)	0.12	49.7
VO_x/SiO_2 (Fresh)	0.04	30.8

Figure 5 shows the soot oxidation rate in plasma-catalytic systems over VO_x/M (M=KIT-6, SBA-15 and SiO_2) catalysts. The soot oxidation rate increases with the progress of the reaction regardless of catalyst type. The soot oxidation rate decreases in the order of VO_x/KIT-6>VO_x/SBA-15>VO_x/SiO_2. During the first 15 min, the soot oxidation rate rises sharply and reaches 90% at 13th min over VO_x/KIT-6. Meanwhile, the soot oxidation rates over VO_x/SBA-15 and VO_x/SiO_2 are only 43% and 30% at 15th min, respectively. The soot oxidation rate over VO_x/KIT-6 and VO_x/SBA-15 reaches 100% at 60th min, which are 7.6% higher than that over VO_x/SiO_2. Figure 6 shows the effect of discharge power on soot oxidation rate and energy efficiency at 30th min over VO_x/M (M=KIT-6 and SiO_2). When the discharge power increases from 16 to 24 W, the soot oxidation rate of VO_x/KIT-6 increases from 75.9% to 100%, while the value increases from 44.0% to 57.9% for VO_x/SiO_2. However, the energy efficiency of VO_x/KIT-6 and VO_x/SiO_2 decreases with the increase of discharge power. At 24 W, the energy efficiency of plasma-catalytic reaction over VO_x/KIT-6 and VO_x/SiO_2 are 0.83 $g \cdot kWh^{-1}$ and 0.48 $g \cdot kWh^{-1}$ lower than that at 16 W.

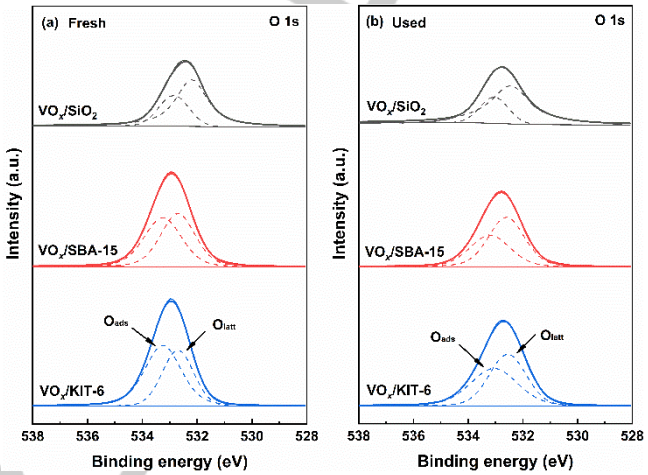

Figure 4. XPS spectra for O 1s of VO_x/M (M=KIT-6, SBA-15 and SiO_2) catalysts: (a) before reaction; (b) after reaction.

The highly energetic electron and chemically reactive species generated by the plasma were the driving force of plasma-induced reactions.[21] The soot particles could react with O· radicals and O_3 in gas phase via Eqs. (1) - (6).[22]

$$C + O \rightarrow CO \quad (1)$$
$$C + 2O \rightarrow CO_2 \quad (2)$$
$$C + O_3 \rightarrow CO + O_2 \quad (3)$$
$$C + 2O_3 \rightarrow CO_2 + 2O_2 \quad (4)$$
$$CO + O \rightarrow CO_2 \quad (5)$$
$$CO + O_3 \rightarrow CO_2 + O_2 \quad (6)$$

Catalyst properties could significantly affect the reaction performance of plasma-catalysis. The S_{BET} and pore volumes of VO_x/KIT-6 and VO_x/SBA-15 are much larger than that of VO_x/SiO_2. Studies have shown that plasma species can be formed in the gas phase and inside the catalyst pore systems with the pore size above 10 μm.[23] As a result, it could be deduced that the plasma-induced electron reaction and the generation of reactive species would occur only in the gas phase. However, the diameters of major chemically reactive species, O· radicals (0.12 nm) and O_3 (0.58 nm), were much smaller than the pore diameter of VO_x/KIT-6 and VO_x/SBA-15, indicating these species could diffuse into the pore systems of the catalysts.[24] The diffusion length of O and O_3 were 51.9 μm and 1.38×10^5 μm, respectively.[25] The relative large diffusion length could contribute to the transport of these species in the catalyst layer and then interact with the catalyst surfaces.[25a] Previous studies indicated that SBA-15 possessed a two-dimensional (2D) hexagonal pore structure, while a three-dimensional (3D) cubic pore structure was observed for KIT-6 samples.[26] The pore structures of the catalyst support would directly affect the performance of catalytic reactions, which was evidenced in catalytic oxidation of formaldehyde and selective oxidation of diphenylmethane.[12, 16b] The 3D mesoporous

structure of KIT-6 would facilitate the diffusion of reactants to the active sites and significantly improve the catalytic activity compared with SBA-15 support with 2D structure.[16b] As with plasma-induced reactions, the 3D mesoporous structure of VO_x/KIT-6 may be more conducive to the diffusion of plasma species inside the pore systems, increasing the probability of effective collisions between radicals, soot particles and catalyst surfaces. As a consequence, the reaction performance could be improved.

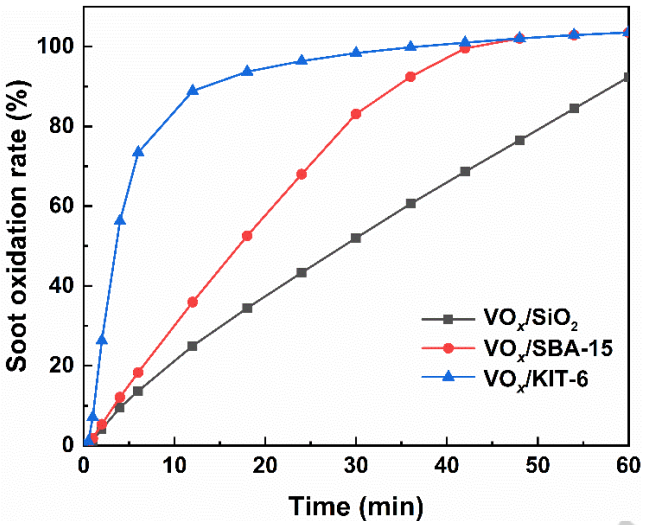

Figure 5. Reaction performance of plasma-catalytic soot oxidation over VO_x/M (M=KIT-6, SBA-15 and SiO_2) catalysts.

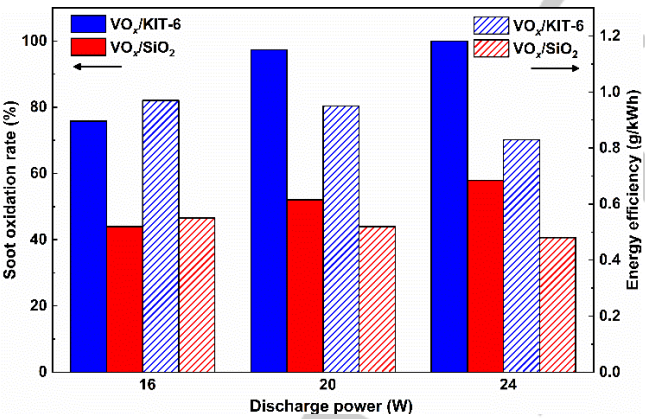

Figure 6. Soot oxidation rate and energy efficiency of the plasma-catalytic process at 30th min as a function of discharge power over VO_x/M (M=KIT-6 and SiO_2) catalysts.

Besides the gas-phase reactions, soot oxidation could also be promoted by the catalyst. It is well known that catalysts with higher S_{BET} could provide more adsorption and active sites for the heterogeneous catalytic reaction. Since catalytic oxidation of soot is a "gas-solid-solid" heterogeneous reaction, the active metal sites on the catalyst surfaces could significantly affect the reaction performance.[3a] The XPS results show that the VO_x/KIT-6 sample possess higher $O_{ads}/(O_{ads}+O_{latt})$ ratio compared to the other samples. The release of surface adsorbed oxygen (O_{ads}) species was much easier on catalysts with higher $O_{ads}/(O_{ads}+O_{latt})$, and contribute to soot oxidation via the soot-catalyst contact points by the transportation of oxygen species. This could also be further confirmed by the H_2-TPR as VO_x/KIT-6 exhibited the best reducibility followed by VO_x/SBA-15 and VO_x/SiO_2 (shown in Table 2). A good correlation between the reaction performance and the reducibility of the catalysts was obtained. The release of O_{ads} could form partially reduced vanadium sites denoted as V(*) (Eqs. 7 and 12), while the consumed surface adsorbed oxygen species could be replenished by the oxygen molecules, plasma-generated O· radicals and O_3, etc (Eqs. 8 - 11).[5] The major reaction mechanisms in the plasma-catalytic systems are as follows:

$$2C + 3V(O) \rightarrow CO + CO_2 + 3V(*) \quad (7)$$

$$O_2(g) + 2V(*) \rightarrow 2V(O) \quad (8)$$

$$O(g) + V(*) \rightarrow V(O) \quad (9)$$

$$O_3(g) + V(*) \rightarrow V(O) + O_2(g) \quad (10)$$

$$OH + V(*) \rightarrow V(O) + H \quad (11)$$

$$CO + V(O) \rightarrow CO_2 + V(*) \quad (12)$$

where V is the surface of vanadium oxides sites, and $V(*)$ is the reduced vanadium oxides sites.

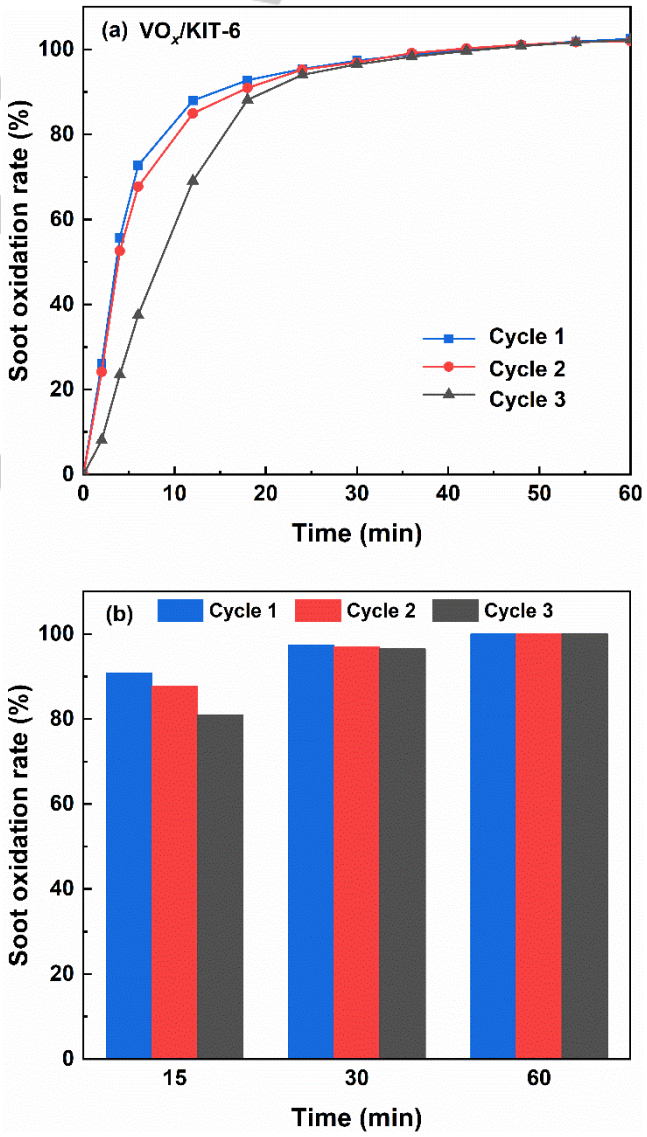

Figure 7. Stability test of VO_x/KIT-6 catalyst for plasma-catalytic soot oxidation.

Stability is an important feature for catalyst performance evaluation, especially in practical applications. The stability test of VO_x/KIT-6 catalyst was performed three consecutive times (Figure 7). Obviously, the soot oxidation rate over VO_x/KIT-6 catalyst decreases slightly with increasing oxidation cycles numbers. After the three cycles, the soot oxidation rate over VO_x/KIT-6 catalyst at 15th min decreases from 90.7% to 80.9%. However, the difference of the soot oxidation rate at 30th min between the first cycle test and the third cycle test is only 0.9%. After an hour of the plasma-catalytic soot oxidation, the soot oxidation rate of all three tests reached 100%. These results indicate that although the reaction rate reduces, the plasma-catalytic system still retains good soot oxidation capacity. Moreover, the result is in consistent with the XPS spectra for O 1s of VO_x/KIT-6 catalyst before and after reaction, as the O_{ads} on the catalyst surface will be consumed gradually during cycle tests, which results in the slight decrease of catalytic activity of VO_x/KIT-6 catalyst.

Conclusion

The experimental results and theoretical analysis showed that pore structure of VO_x/M (M=KIT-6, SBA-15 and SiO_2) catalysts affects plasma-catalytic soot oxidation. VO_x/KIT-6 exhibited the highest soot oxidation rate in plasma-catalytic system. The S_{BET}, XRD and TEM results revealed that VO_x/KIT-6 and VO_x/SBA-15 had large specific surface areas and good dispersion of vanadium species. The H_2-TPR and XPS results indicated that VO_x/KIT-6 exhibited the highest reducibility and $O_{ads}/(O_{ads}+O_{latt})$ ratio followed by VO_x/SBA-15 and VO_x/SiO_2. The well-developed 3D mesoporous structure of VO_x/KIT-6 contributed to the transportation and diffusion of reactive species, including radicals and oxygen species. The improved properties of VO_x/KIT-6 were also attributed to the large amounts of active sites and surface adsorbed oxygen species on the surface of catalyst, which resulted in excellent performance in plasma-catalytic soot oxidation.

Supporting Information Summary

The supporting information includes the details in catalyst preparations, experimental setup, catalyst characterizations, XRD patterns and XPS parameters of the used catalysts.

Acknowledgements

The work was supported by National Natural Science Foundation of China (No.51976093) and K.C. Wong Magna Fund in Ningbo University.

Keywords: KIT-6 • Mesoporous structure • Plasma-catalysis • Soot oxidation • Vanadium

[1] M. A. Mokhri, N. R. Abdullah, S. A. Abdullah, S. Kasalong, R. Mamat, *Procedia Eng.* **2012**, *41*, 1750-1755.

[2] X. Mei, J. Xiong, Y. Wei, C. Wang, Q. Wu, Z. Zhao, J. Liu, *Chin. J. Catal.* **2019**, *40*, 722-732.

[3] a) L.-J. Liu, X.-X. Li, H. Wang, B. Xue, X.-M. Zheng, M. Chen, *RSC Adv.* **2015**, *5*, 40012-40017; b) Y. Sekine, H. Koyama, M. Matsukata, E. Kikuchi, *Fuel* **2013**, *103*, 2-6.

[4] M. Fu, J. Lin, W. Zhu, J. Wu, L. Chen, B. Huang, D. Ye, *J. Rare Earths* **2014**, *32*, 153-158.

[5] H. Ranji-Burachaloo, S. Masoomi-Godarzi, A. A. Khodadadi, Y. Mortazavi, *Appl. Catal. B Environ.* **2016**, *182*, 74-84.

[6] a) D. W. Kwon, D. H. Kim, S. Lee, J. Kim, H. P. Ha, *Appl. Catal. B Environ.* **2021**, *289*, 120032; b) N. Mizuno, K. Kamata, *Coord. Chem. Rev.* **2011**, *255*, 2358-2370.

[7] P. Selvam, T. A. Paulose, *J. Nanosci. Nanotechnol.* **2006**, *6*, 1758-1764.

[8] X. Zhu, Y. Yang, X. Geng, C. Zheng, J. Zhou, X. Gao, Z. Luo, M. Ni, K. Cen, *IEEE Trans. Plasma Sci.* **2016**, *44*, 3379-3385.

[9] J. Liu, Z. Zhao, C. Xu, A. Duan, L. Zhu, X. Wang, *Catal. Today* **2006**, *118*, 315-322.

[10] T. Tsoncheva, G. Issa, J. M. López Nieto, T. Blasco, P. Concepcion, M. Dimitrov, G. Atanasova, D. Kovacheva, *Microporous Mesoporous Mater.* **2013**, *180*, 156-161.

[11] B. Sridevi, P. Nagaiah, A. H. Padmasri, B. David Raju, K. S. Rama Rao, *J. Chem. Sci.* **2017**, *129*, 601-608.

[12] J. Liu, F. Qin, Z. Huang, L. Huang, Z. Liao, H. Xu, W. Shen, *Catal. Lett.* **2019**, *149*, 1894-1902.

[13] H. Lan, Q. Yao, Y. Zhou, B. Zhang, Y. Jiang, *Mol. Catal.* **2020**, *498*, 111279.

[14] H. Lan, X. Xiao, S. Yuan, B. Zhang, G. Zhou, Y. Jiang, *Catal. Lett.* **2017**, *147*, 2187-2199.

[15] M. Hussain, F. A. Deorsola, N. Russo, D. Fino, R. Pirone, *Fuel* **2015**, *149*, 2-7.

[16] a) Y. Liu, W. Feng, T. Li, H. He, W. Dai, W. Huang, Y. Cao, K. Fan, *J. Catal.* **2006**, *239*, 125-136; b) D. Santhanaraj, C. Suresh, A. Selvamani, K. Shanthi, *New J. Chem.* **2019**, *43*, 11554-11563; c) P. Ji, X. Gao, X. Du, C. Zheng, Z. Luo, K. Cen, *Catal. Sci. Technol.* **2016**, *6*, 1187-1194.

[17] L. Jiang, Q. Liu, G. Ran, M. Kong, S. Ren, J. Yang, J. Li, *Chem. Eng. J.* **2019**, *370*, 810-821.

[18] F. He, J. Luo, S. Liu, *Chem. Eng. J.* **2016**, *294*, 362-370.

[19] T. Chang, J. Lu, Z. Shen, Y. Huang, D. Lu, X. Wang, J. Cao, R. Morent, *Appl. Catal. B Environ.* **2019**, *244*, 107-119.

[20] B. Wang, C. Chi, M. Xu, C. Wang, D. Meng, *Chem. Eng. J.* **2017**, *322*, 679-692.

[21] V. Palma, M. Cortese, S. Renda, C. Ruocco, M. Martino, E. Meloni, *Nanomaterials (Basel)* **2020**, *10*, 1596.

[22] a) T. Kuwahara, S. Nishii, T. Kuroki, M. Okubo, *Appl. Energy* **2013**, *111*, 652-656; b) M. Okubo, N. Arita, T. Kuroki, K. Yoshida, T. Yamamoto, *Plasma Chem. Plasma P.* **2008**, *28*, 173-187; c) K. Yoshida, *IEEE Trans. Ind. Appl.* **2019**, *55*, 5261-5268.

[23] Y.-R. Zhang, K. Van Laer, E. C. Neyts, A. Bogaerts, *Appl. Catal. B Environ.* **2016**, *185*, 56-67.

[24] a) I. Tsukada, S. Higuchi, *Jpn. J. Appl. Phys.* **2004**, *43*, 5307-5312; b) J. C. Slater, *J. Chem. Phys.* **1964**, *41*, 3199-3204.

[25] a) H.-H. Kim, Y. Teramoto, N. Negishi, A. Ogata, *Catal. Today* **2015**, *256*, 13-22; b) R. Ono, Y. Yamashita, K. Takezawa, T. Oda, *J. Phys. D: Appl. Phys.* **2005**, *38*, 2812-2816.

[26] J. Hochstrasser, A. Svidrytski, A. Holtzel, T. Priamushko, F. Kleitz, W. Wang, C. Kubel, U. Tallarek, *Phys. Chem. Chem. Phys.* **2020**, *22*, 11314-11326.

Entry for the Table of Contents

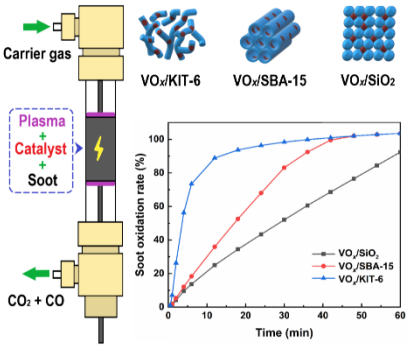

VO_x/M (M=KIT-6, SBA-15 and SiO_2) catalysts were synthesized by impregnation method and used for soot oxidation with plasma. VO_x/KIT-6 exhibited the highest soot oxidation rate and its well-developed 3D mesoporous structure benefited the transportation and diffusion of reactive species (O· radicals and O_3).